

Ab initio calculation of Hubbard parameters for Rydberg-dressed atoms in an one-dimensional optical lattice

Yashwant Chougale and Rejish Nath

Indian Institute of Science Education and Research, Pune 411 008, India

Abstract. We obtain *ab initio* the Hubbard parameters for Rydberg-dressed atoms in an one-dimensional sinusoidal optical lattice in the basis of maximally localized wannier states. Finite range, soft-core inter-atomic interactions become the trait of Rydberg admixed atoms, which can be extended over many neighbouring lattice sites. On contrary to dipolar gases, where the interactions follow an inverse cubic law, the key feature of Rydberg-dressed interactions being the possibility of making neighbouring couplings to the same magnitude as that of the onsite ones. The maximally localized Wannier functions are typically calculated via spread minimization procedure [Phys. Rev. B **56**, 12847 (1997)] and always found to be real functions apart from a trivial global phase when considering an isolated set of Bloch bands. For an isolated single Bloch band, the above procedure reduces to a simple quasi-momentum dependent unitary phase transformation. Here, in stead of minimizing the spread, we employ a diagonal phase transformation which eliminates the imaginary part of the Wannier functions. The resulting Wannier states are found to be maximally localized and in exact agreement with those obtained via spread minimization procedure. Using that we calculate the Hubbard couplings from the Rydberg-admixed interactions, including dominant density assisted tunnelling coefficients. In the end we provide realistic lattice parameters for the state of the art experimental Rydberg dressed Rubidium setup.

Submitted to: *J. Phys. B: At. Mol. Phys.*

Contents

1 Introduction 2

2 Rydberg dressed atoms in an one-dimensional optical lattice 4

2.1 The atom-lattice setup and Rydberg-Rydberg interactions 4

2.2 Many body Hamiltonian and the extended Hubbard model 5

3 Maximally localized Wannier functions 6

4 Hubbard Parameters 7

4.1 Hopping and short-range interaction parameters 7

4.2 Rydberg admixed potential: density-density interactions 9

4.3 Rydberg admixed potential: density assisted tunnelings 12

4.4 An example: Rubidium atoms 13

5 Conclusion 13

6 Acknowledgements 14

Appendices 15

1. Introduction

A new wave of study has emerged in cold Rydberg atom-community along the lines of so-called *Rydberg-dressed atoms* [1, 2, 3, 4, 5, 6, 7]. They are mostly the ground state atoms with a very tiny fraction of Rydberg excited ones, represented by the state vectors of the form $\sim |g\rangle + \alpha|r\rangle$ with $|\alpha| \ll 1$, where $|g\rangle$ and $|r\rangle$ are respectively the ground and Rydberg states. Rydberg excited atoms are known to exhibit prodigious inter-atomic interactions [9] that can suppress further excitations within a finite volume, called the Rydberg blockade [10, 11, 12]. Though the excitations are short lived, the huge interactions made it feasible to study certain interesting many body effects, within the frozen gas limit [13, 14, 15, 16, 17, 18, 19]. Later, Rydberg admixing turned up as a remedy to overcome the life time constraint of Rydberg excited atoms, especially augmented its effective life time by a factor of $1/|\alpha|^2$. Inter-atomic interactions with a softcore potential barrier [5] becomes the trait of Rydberg dressed atoms and is verified very recently in an experiment done with two atoms trapped using optical tweezers [20]. In a short span of time, it has led to various exciting studies: in quantum many body physics [5, 21, 22, 23, 24, 25, 26, 27] including frustrated quantum magnets [28, 29], quantum computing [30, 31, 32] and spin squeezing for metrology [33, 34]. As lately proposed, an electro-magnetically induced transparency based Rydberg dressing scheme utilizing metastable states of Alkaline earth atoms may help to achieve enhanced atomic interactions even with longer coherence times [35].

The quantum simulation of many body physics predominantly rely on ultra cold atoms loaded in optical lattices [36, 37] described by local Hubbard models [38]. The Bose-Hubbard model (BHM) with contact interactions and nearest neighbour hoppings, forms the paradigmatic example of a system exhibiting quantum phase transition, dating back to the prediction of superfluid-mott insulator transition by Fisher *et. al* [39] and for the first time it is observed in a cold atom-lattice setup [40]. Due to the tremendous progress in experimental techniques, in particular, the ability to address a single atom in a lattice site [41, 42, 43] as well as to describe the experimental results quantitatively accurate it is required to calculate the Hubbard parameters in a basis of highly localized single particle states. An example being the basis of maximally localized Wannier states, can be obtained by unitary mixing of the Bloch states [44, 45]. In a seminal work by Marzari and Vanderbilt [46], they showed how to calculate the maximally localized Wannier functions (MLWFs) by minimizing the spread of generalized Wannier states. Their approach has been employed successfully in studying complex solid state materials [47], and recently been employed for cold atoms in optical lattices [48]. When lattice depths are sufficiently large, tight binding together with harmonic approximation is in good agreement with MLWF calculations for lowest isolated bands.

The well-acclaimed BHM is then generalized to systems with long-range interactions (e.g. magnetic atoms, polar molecules or atoms with laser-induced interactions) termed as an extended BHM (EBHM) [49, 50] in which the interactions between neighbouring sites are included. EBHM is predicted to be abundant with exotic quantum phases such as stripes, checkboard phases, supersolids, Haldane insulators etc [51, 52, 53, 54, 55, 56]. Lately, it has been demonstrated and experimentally probed using magnetic Erbium atoms trapped in a 3D optical lattice [57]. Here, we derive the EBHM in a 1D lattice of Rydberg admixed atoms from first principle and as we show it has certain advantages over dipolar systems. Among them, the most striking property is the possibility of engineering the strengths of off-site couplings to same magnitude as that of onsite ones, hence position independent. This may have far reaching consequences in the context of quantum many body physics [59] especially in frustrated magnetism [28, 29].

An additional correlated feature of interacting lattice gases is the density assisted inter-site or inter-band tunneling, in which the former has been observed in atoms with both contact interactions [58] and long-range dipolar interactions [57]. Termed as bond-charge interaction in the context of fermions, the density assisted tunneling (DAT) strongly influences the MOT insulator-superfluid transition points in bosonic and Bose-Fermi mixtures [60]. It may also lead to novel quantum phases for polar molecules in optical lattices [61].

Here, we calculate *ab initio* the Hubbard parameters in the basis of MLWFs for an extended Hubbard model implemented using Rydberg dressed atoms in an one-dimensional sinusoidal optical lattice. Motivated by the hypothesis that MLWFs are real functions apart from a trivial global phase, we implement a diagonal $U(1)$ phase transformation for the Bloch states which eliminate the imaginary part of the Generalized Wannier states. The resulting Wannier states are found to be maximally

localized and in exact agreement with those obtained via spread minimization procedure. We estimate the Hubbard parameters including the DAT coefficients and discuss their properties within the two lowest Bloch bands and up to second nearest neighbour couplings for Rydberg admixed interaction potential.

The paper is structured as follows: in section 2 we discuss the Rydberg-lattice setup, the governing many body Hamiltonian and derive *ab initio* the extended Hubbard model in the maximally localized Wannier basis. In section 3 we discuss how MLWFs are calculated using a unitary diagonal phase transformation in the isolated Bloch bands for a sinusoidal 1D optical lattice potential. The results for the Hubbard parameters are discussed in section 4 as well as we provide realistic numbers for the state of the art experimental Rubidium lattice setup 4.4. Finally we conclude in section 5.

2. Rydberg dressed atoms in an one-dimensional optical lattice

2.1. The atom-lattice setup and Rydberg-Rydberg interactions

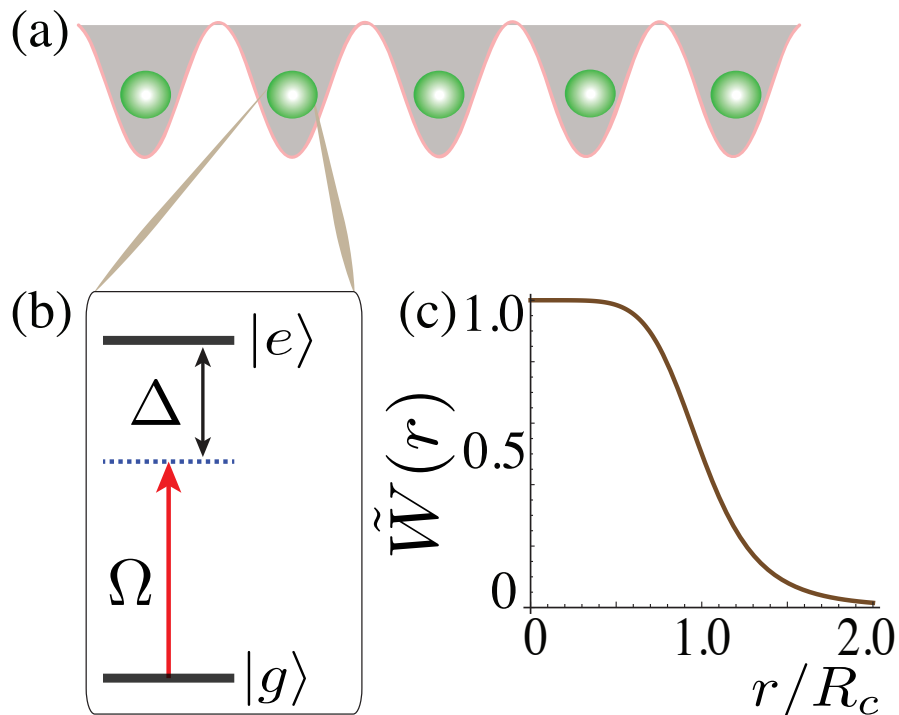


Figure 1. (a) The one-dimensional lattice setup with Rydberg dressed atoms. (b) The two-level scheme which consists of a ground state $|g\rangle$ being weakly coupled to a Rydberg state $|e\rangle$ by a laser field with detuning Δ and Rabi frequency Ω . (c) The emerging inter-atomic interactions between the dressed ground state atoms: $\tilde{W}(r) = W(r)/W_0$, where $W_0 = (\Omega/2|\Delta|)^4 C_6$ as a function of interparticle separation r .

We consider bosonic atoms loaded in an one-dimensional optical lattice of potential $V_{OL}(x) = V_0 \sin^2(k_0 x)$, where V_0 is the lattice depth and wave number $k_0 = \pi/d$ with

d being the lattice spacing. The ground state $|g\rangle$ of the atoms are weakly admixed to an excited Rydberg state $|e\rangle$ using optical fields, see Figure 1. Two atoms with an inter-atomic separation r , occupying the state $|e\rangle$ experience an interaction potential of the form C_6/r^6 , where the van der Waal (vdW) dispersion co-efficient $C_6(\propto n^{11})$ can be either spatially isotropic or anisotropic [28, 25] depending on different angular momentum quantum numbers $\{l, j, m_j\}$ of the Rydberg state $|e\rangle \equiv |n, l, j, m_j\rangle$, where n is the principal quantum number. The above vdW interactions between the Rydberg excited atoms lead to a tunable soft-core potential for the atoms in the admixed state (see Figure 1c) and is

$$W(r_{ij}) = \left(\frac{\Omega}{2|\Delta|} \right)^4 \frac{C_6}{(r_{ij}^6 + R_c^6)}, \quad (1)$$

where Δ is the detuning and Ω is the rabi frequency with respect to the $|g\rangle$ - $|r\rangle$ atomic transition. The parameter, $R_c = [C_6/2\hbar|\Delta|]^{1/6}$ being the Condon radius determines the range of the interactions and r_{ij} is the spatial separation between i^{th} and j^{th} atoms. The Rydberg blockade effect is apparent at distances $r_{ij} \leq R_c$, where the interaction potential is saturated to a constant value provided by the light shift of the blockaded atoms [5, 20]. For large values of $r_{ij} > R_c$, we retrieve the vdW type interactions, $W(r_{ij}) \approx \tilde{C}_6/r_{ij}^6$ with a reduced vdW coefficient $\tilde{C}_6 = (\Omega/2|\Delta|)^4 C_6$. Notably the range of the interactions $\sim R_c$ can be extended over several lattice sites by regulating the detuning Δ or the interaction coefficient C_6 , fabricating the scenario identical to that of long-range interacting systems such as magnetic atoms or polar molecules [50, 57, 61].

2.2. Many body Hamiltonian and the extended Hubbard model

Our starting point is the second quantization many-body Hamiltonian for a gas of interacting bosons in an external potential $V_{OL}(\mathbf{r})$:

$$\hat{H} = \int d\mathbf{r} \hat{\Psi}^\dagger(\mathbf{r}) \hat{h}_0 \hat{\Psi}(\mathbf{r}) + \frac{1}{2} \int d\mathbf{r} \int d\mathbf{r}' \hat{\Psi}^\dagger(\mathbf{r}) \hat{\Psi}^\dagger(\mathbf{r}') U_I(\mathbf{r} - \mathbf{r}') \hat{\Psi}(\mathbf{r}) \hat{\Psi}(\mathbf{r}') \quad (2)$$

where the field operator $\hat{\Psi}(\mathbf{r})$ [$\hat{\Psi}^\dagger(\mathbf{r})$] annihilates [creates] a boson at the position \mathbf{r} . The term $\hat{h}_0 = -\hbar^2 \Delta^2 / 2m + V_{OL}(\mathbf{r})$ corresponds to the single particle Hamiltonian. The two-particle interactions are, $U_I(\mathbf{r} - \mathbf{r}') = U(\mathbf{r} - \mathbf{r}') + W(\mathbf{r} - \mathbf{r}')$ with the first term being the typical contact interactions: $U(\mathbf{r} - \mathbf{r}') = g\delta(\mathbf{r} - \mathbf{r}')$ characterized by the parameter, $g = 4\pi\hbar^2 a/m$ where a is the s -wave scattering length, and the second term is the interaction potential among the Rydberg-admixed atoms. Next, we expand the field operators in the basis of maximally localized single particle Wannier functions $w_n(\mathbf{r} - \mathbf{R}_j)$ (see section 3) centered around each lattice site at $\mathbf{R}_j = j\mathbf{R}$ and the lattice vector \mathbf{R} is such that $V(\mathbf{r} + \mathbf{R}) = V(\mathbf{r})$. Hence, the field operator

$$\hat{\Psi}(\mathbf{r}) = \sum_j \sum_n w_n(\mathbf{r} - \mathbf{R}_j) \hat{a}_{jn}, \quad (3)$$

where \hat{a}_{jn} (\hat{a}_{jn}^\dagger) annihilates (creates) a boson in the mode represented by the Wannier function $w_n(\mathbf{r} - \mathbf{R}_j)$ at j^{th} lattice site. They satisfy the commutation relation $[\hat{a}_{in}, \hat{a}_{jm}] =$

$\delta_{ij}\delta_{nm}$. Inserting the above expression for field operator in Equation 2, we arrive at a general extended Hubbard model:

$$\hat{H} = - \sum_{i,j} \sum_{n,m} J_{ij}^{nm} \hat{a}_{in}^\dagger \hat{a}_{jm} + \frac{1}{2} \sum_{i,j,i',j'} \sum_{n,m,n',m'} (U_I)_{ij i' j'}^{nm n' m'} \hat{a}_{in}^\dagger \hat{a}_{jm}^\dagger \hat{a}_{j'm'} \hat{a}_{i'n'} \quad (4)$$

where the hopping and the interaction matrix elements are respectively

$$J_{ij}^{nm} = - \int d\mathbf{r} w_n^*(\mathbf{r} - \mathbf{R}_i) [-\hbar^2 \Delta^2 / 2m + V_{OL}(\mathbf{r})] w_m(\mathbf{r} - \mathbf{R}_j) \quad (5)$$

$$(U_I)_{ij i' j'}^{nm n' m'} = \iint d\mathbf{r} d\mathbf{r}' w_n^*(\mathbf{r} - \mathbf{R}_i) w_m^*(\mathbf{r}' - \mathbf{R}_j) U_I(\mathbf{r} - \mathbf{r}') w_{m'}(\mathbf{r}' - \mathbf{R}_{j'}) w_{n'}(\mathbf{r} - \mathbf{R}_{i'}). \quad (6)$$

The subscripts and superscripts in J and U_I represent the lattice site and band indices respectively. In cold atoms, it can be the case that interaction and kinetic energies are smaller than the lattice depth V_0 , then the summation over the band indices is truncated beyond few lowest Bloch bands. Below we calculate the microscopic parameters for the EBHM (equation 4) upto next nearest neighbour couplings with in the two lowest Bloch bands for the 1D lattice setup.

3. Maximally localized Wannier functions

The generalized Wannier functions are calculated by the unitary mixing of N degenerate or closely spaced Bloch eigenstates and in 1D it is written as,

$$w_n(x - X_j) = \frac{d}{2\pi} \int_{BZ} dq e^{-iqX_j} \sum_{m=1}^N U_{nm}(q) \psi_q^m(x), \quad (7)$$

where $\psi_q^m(x)$ is the Bloch function for the m^{th} Bloch band for a quasi-momentum q . The operator $U_{nm}(q) \in U(N)$ is an unitary matrix satisfying the periodic boundary condition in the momentum space: $U_{nm}(q + 2q_B) = U_{nm}(q)$ with $q_B = \pi/d$ and N corresponds to the number of lattice sites in the unit cell. BZ indicates that the integration is carried over the first Brillouin zone. As proposed in a seminal paper, the MLWFs can be obtained from generalized Wannier functions by obtaining $U_{nm}(q)$ which minimizes the spread functional [45]:

$$\Omega = \sum_{n=1}^N [\langle 0n|x^2|0n\rangle - \langle 0n|x|0n\rangle^2], \quad (8)$$

where $\langle x|jn\rangle = w_n(x - X_j)$. MLWFs are shown to be exponentially localized [44, 62] and they provide the best optimal basis for estimating Hubbard parameters. For an isolated single Bloch band ($N = 1$), the unitary transformation is an abelian $U(1)$ gauge transformation and, is nothing but an update for the phase of Bloch functions i.e. $\psi_q^m \rightarrow e^{i\phi_q^m} \psi_q^m$. It is also the case for the setup we considered here. Thus, once the Bloch spectrum (see Appendix A) is found, the problem for calculating MLWFs reduces to finding the phases ϕ_q^m which minimize the spread Ω . It has been shown that the results obtained by minimizing the Wannier spread for isolated Bloch bands are same as the exponentially localized wannier functions discussed by Kohn [44]. Writing the

Wannier spread as a sum of gauge independent and dependent terms: $\Omega = \Omega_I + \tilde{\Omega}_D$, with subsequent division of gauge dependent one to diagonal and off-diagonal terms: $\tilde{\Omega}_D = \Omega_d + \Omega_{od}$. For an isolated band Ω_{od} vanishes and the question reduces to finding the unitary transformation which eliminates Ω_d [45]. Note that, there also exists other localization procedures for Wannier states e.g. maximizing the sum of Coulomb self energies [63].

Here we do not employ the minimization of Wannier spread, rather make use of the conjecture that MLWFs are real functions upto a global phase factor. In our case ($N = 1$) the generalized Wannier functions are

$$w_n(x - X_j) = \frac{d}{2\pi} \int_{BZ} dq e^{-iqX_j} e^{i\phi_q^n} \psi_q^n(x). \quad (9)$$

The periodic Bloch functions $\psi_q^n(x)$ are calculated as prescribed in [Appendix A](#). The phases ϕ_q^n for the unitary transformation is obtained by minimizing the absolute value of the imaginary part of the Wannier function in equation 9 and it leads to

$$\phi_q^n = \arctan \left(\frac{\Re[u_q^n(x_0)]}{\Im[u_q^n(x_0)]} \right) - kx_0. \quad (10)$$

In our numerics, for symmetric $u_q^n(x)$ we took $x_0 = 0$ and for anti-symmetric $u_q^n(x)$ we took the point at which the imaginary part of $u_q^n(x)$ is maximum. The resulting Wannier functions match perfectly with those obtained via spread minimization procedure []. As an example, MLWFs for the two lowest bands ($n = 1, 2$) in a 1D sinusoidal lattice are shown in figure 2a for $V_0 = 10E_R$ and their exponential localization is conspicuous in the log scale plot of the vertical axis.

4. Hubbard Parameters

4.1. Hopping and short-range interaction parameters

We briefly summarize the behaviour of Hopping (J) and contact interaction (U) matrix elements as a function of lattice depth V_0 calculated using MLWFs (see figure 2). The spatial spread of Wannier functions $w_n(x)$ gets larger and larger as we go higher in bands (n) and for a given n it decreases with increasing V_0 . The localization properties of $w_n(x)$ are critical in determining the behaviour of J and U . For instance, the nearest neighbour hopping ($J_n^0 = J_{12}^{nn}$) is larger in second band compared to that in the first one. Also for both bands it decreases exponentially with increasing V_0 [figure 2(b)]. The next nearest neighbour hopping is two orders of magnitude less than J_n and is safely disregarded in the (E)BHM. Note that there is no inter-band hopping due to the orthogonality property of Wannier functions. The results from WKB approximation for the lowest (J_1^0) is shown in dotted line in 2(b)] and is in good agreement with that of exact results.

Since $w_n(x)$ gets more and more localized with larger values of V_0 , the onsite interactions ($U_0^n = U_{0000}^{nnnn}$) for any n increases as a function of V_0 [figure 2(c)]. As expected, the behaviour for the nearest neighbour interactions ($U_1^n = U_{0101}^{nnnn}$) is just

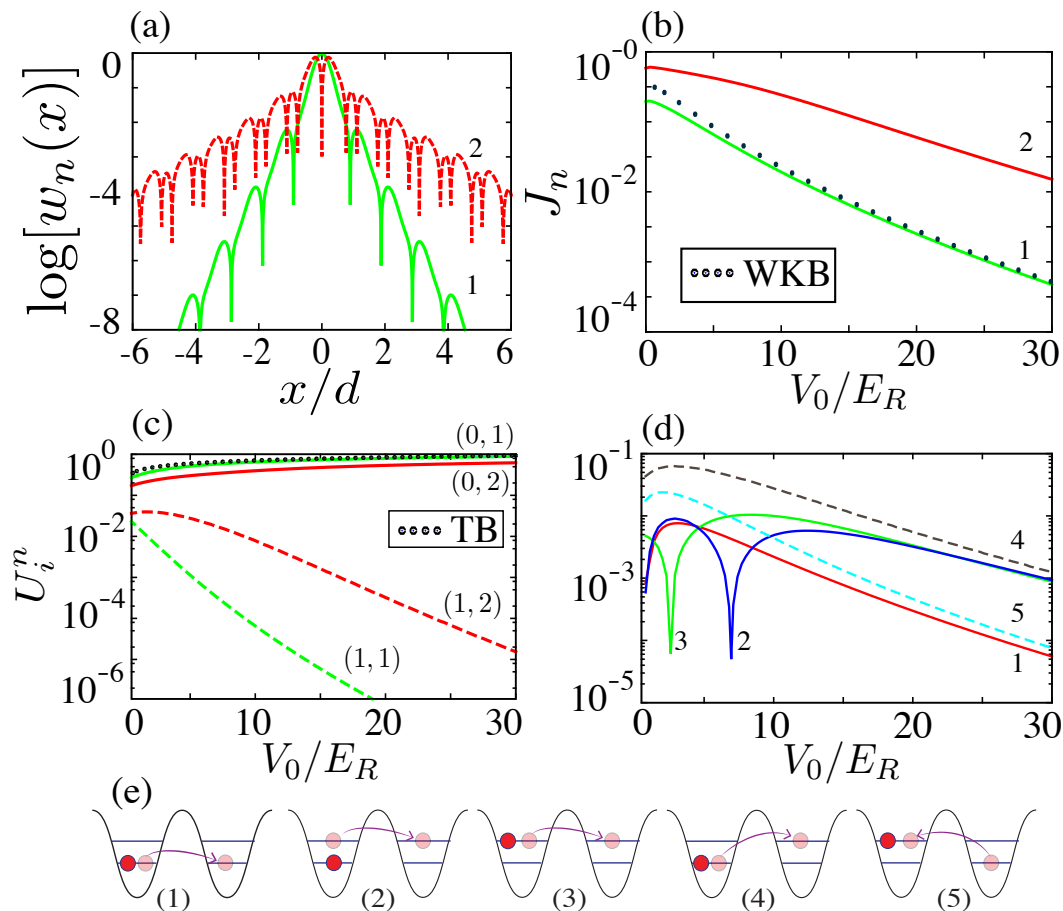


Figure 2. (a) The maximally localized Wannier functions $w_n(x)$ for the two lowest Bloch bands in a 1D sinusoidal optical lattice with $V_0 = 10E_R$. The exponential decay of MLWFs are clearly visible with a log-scale along the y -axis. (b) The nearest neighbour hopping parameter $J_n = J_{12}^{nn}$ (see equation. 5) for the two lowest bands as a function of lattice depth V_0 . As expected, the hopping get suppressed as V_0 becomes larger and larger. Note that Higher the band index larger the hopping matrix element for a given V_0 as evident from the Wannier functions that their spatial extension increases with n . For $n = 1$, the results from the WKB approximation (dotted line) is in good agreement, but for higher bands (not shown) they differ considerably. The band indices for figures (a) and (b) are shown at the corresponding plots. (c) The on-site (solid lines and $i = 0$) and nearest neighbour (dashed lines and $i = 1$) short range interaction parameters ($U_i^n = U_{iii}^{nnnn}$) for the two lowest bands ($n = 1, 2$). Onsite interaction is higher for the lowest band and the nearest neighbour interactions are opposite to it. The results from the tight-binding approximation is shown in the dotted line. (d) shows the scaled (units of \tilde{g}) DAT amplitudes as a function of V_0 , which include DAT with in bands to the nearest neighbour site (solid lines) and those between bands to the nearest neighbour site (dashed lines). The different DAT processes are shown in (e) and the corresponding plots are indicated by the same numbers in (d).

opposite and also few orders of magnitude lower than that of the onsite ones, which may hardly affect the many body phase diagram of BHM. On the other hand, the different DAT matrix elements shown in figure 2(d), though their magnitudes are relatively small (has to be compared with hopping amplitudes J_n) some of them may significantly modify the dynamics in BHM [58], even in sufficiently strong optical lattices. In particular, if restricted in the lowest band the dominant off-site contribution in BHM comes from a DAT term [first processes in figure 2(e)] of the form $\sim \sum_{\langle ij \rangle} \hat{a}_i^\dagger (\hat{n}_i + \hat{n}_{i+1}) \hat{a}_{i+1}$ and is explicitly occupation dependent. The signatures of this term in a deep MOT state are probed in a recent experiment using tilted optical lattices [58]. In figure 2(d) only the dominant DAT coefficients are shown and corresponding processes are depicted in figure 2(e). Note that onsite inter-band tunnelings are prohibited by the orthogonality property of MLWFs. With the inclusion of DAT terms in the discrete lattice Hamiltonian, the model is now generally termed as *non-standard* BHM.

4.2. Rydberg admixed potential: density-density interactions

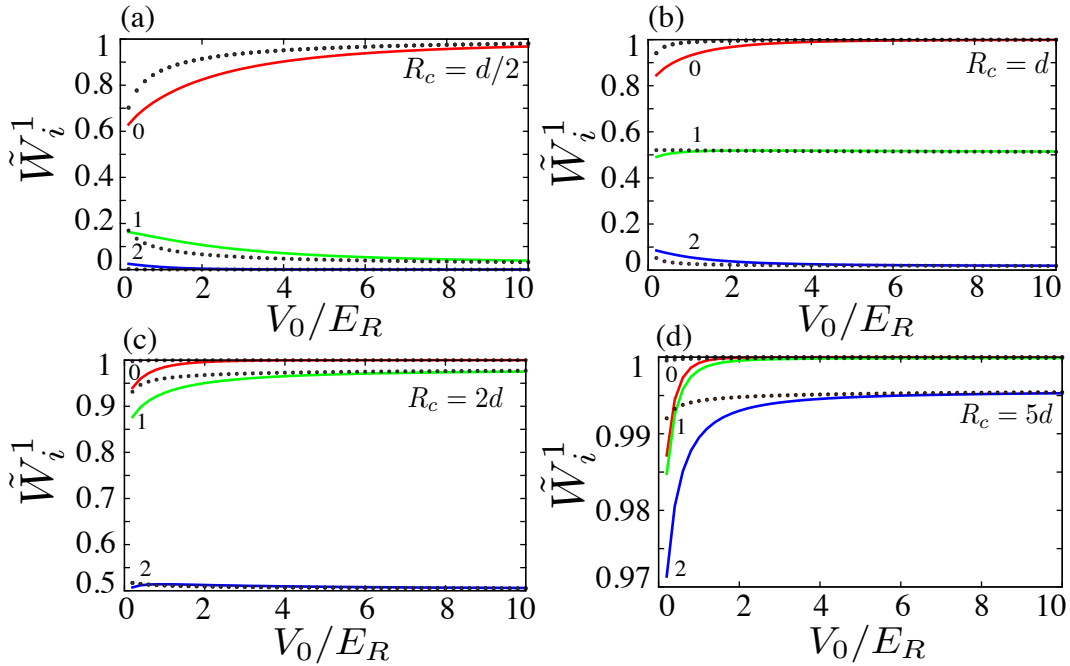


Figure 3. The Rydberg admixed interaction parameters $\tilde{W}_i^{-1} = W_{00ii}^{1111}/W_{eff}$ in the lowest band ($n = m = 1$) as a function of the lattice depth V_0 with (a) $R_c = d/2$, (b) $R_c = d$, (c) $R_c = 2d$ and (d) $R_c = 5d$. The onsite ($i = 0$), nearest neighbour ($i = 1$) and next nearest neighbour ($i = 2$) interaction couplings are shown, indicated by the numbers in the plot. As R_c increases, the off-site matrix elements become significant as that of onsite ones. This arises from the flattened nature of the soft-core barrier of the Rydberg induced potential. In addition, they all saturate to the same value independent of the separation between the atoms as R_c becomes larger and larger. The results from the tight binding approximation are shown in dotted lines.

We rewrite the binary interaction (equation 1) between the Rydberg admixed atoms as

$$W(r_{ij}) = \frac{W_{eff}}{[(r_{ij}/R_c)^6 + 1]}, \quad (11)$$

with $W_{eff} = \hbar\Omega^4/(8|\Delta|^3)$ being an effective interaction strength given by the light shift due to the Rydberg laser and $R_c = [C_6/2\hbar|\Delta|]^{1/6}$ provides the interaction range. Among the two parameters, R_c can be controlled independently of W_{eff} by changing the Rydberg state through $C_6(n)$, but any variation in Δ and Ω affects both simultaneously. The possibility of tuning the interaction range without affecting the effective strength can be pointed out as an elite feature of Rydberg admixed atoms compared to other existing long-range systems. See section. 4.4 for the values of R_c as a function of $C_6(n)$ (or simply n) for Rubidium atoms.

With this, we estimate the Hubbard parameters for Rydberg-dressed interaction ($W_{ij'i'j'}^{nmm'm'}$) using MLWFs, as a function of both lattice depth V_0 and R_c . The results for the lowest band ($\tilde{W}_i^1 = W_{00ii}^{1111}/W_{eff}$) is shown in figure 3. For any value of R_c , the onsite interaction ($i = 0$) increases with increasing V_0 but it saturates rather quickly compared to that of short-range interactions for sufficiently large values of R_c . This is attributed to the flat nature of the softcore potential. The behaviour of off-site matrix elements with V_0 depends crucially on the value of R_c . For instance, for $R_c = d/2$ all of them decreases with V_0 and become negligible for sufficiently large V_0 [figure 3(a)]. When $R_c \sim d$, the character of the nearest neighbour ($i = 1$) coupling changes and it increases with V_0 [figure 3(b)]. For $R_c \sim 2d$ it becomes almost identical to that of the onsite interaction [figure 3(c)] and in addition the next nearest neighbour coupling becomes significantly large, becomes half of onsite and first nearest neighbour interactions. As shown in figure 3(d) for $R_c = 5d$ all the three are almost same in magnitude. Hence, as R_c increases the off-site matrix elements become as relevant as onsite interactions. The same results for the first excited band is shown in figure. 4 and that of when one atom occupying the lowest band and the second in the first excited band is shown in figure. 5. In all cases, the tight binding results are shown in dotted lines.

The important properties to be noted as follows: first point is that due to the flattened nature of the Rydberg potential at short distances, the dominant matrix elements for the density-density interactions saturate quickly to W_{eff} as a function of V_0 when $R_c > d$. This can be seen again as a unique feature of Rydberg dressed interactions compared to other inter-atomic potentials. This is because the potential $W(x - x')$ changes hardly over an inter-particle distance of $x - x' \sim R_c$, hence it can be approximated to a constant such that

$$W_{0i0i}^{nmmnm} \simeq W(x - x') \int dx |w_n^*(x)|^2 \int dx' |w_m^*(x' - X_i)|^2 = W_{eff}. \quad (12)$$

As we go higher in the bands, the saturation behaviour with V_0 slows down. It can also be seen as that the saturation occurs when the MLWFs are fully accommodated inside the soft-core barrier of the potential or when $\Omega < R_c$ and it delays the saturation as a function of V_0 for higher bands. The second point is that nearest neighbouring

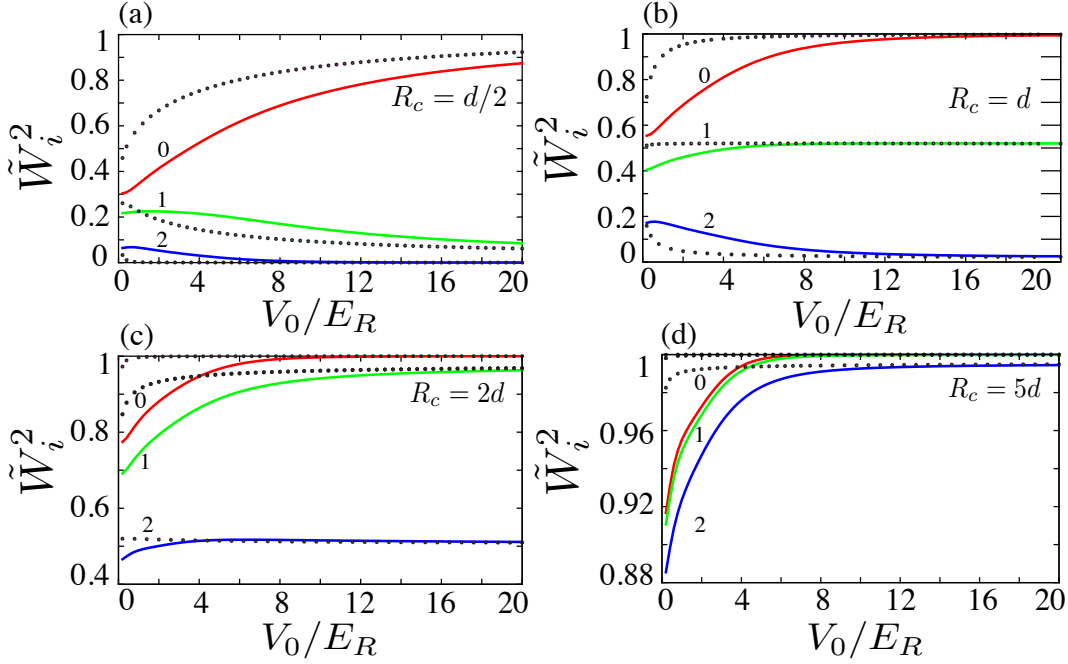


Figure 4. The same as in figure 3, but for the first excited band ($\tilde{W}_i^2 = W_{00ii}^{2222}/W_{eff}$). The results from tight binding approximation are shown by the dotted lines. The value of i is used in labelling the plots.

interactions can be made same strength as that of onsite interactions by adjusting the value of R_c i.e. they become position-independent. This may have far-reaching consequences in the context of many body physics [59], and in particular on frustrated magnetism [28, 29]. Since R_c is varied through vdW coefficient C_6 , the different many body quantum phases arising from the long-range nature of the interactions can be accessed simply as a function of the principal quantum number n without changing other parameters in the system. The quantitative details for a Rubidium lattice setup is worked out in section. 4.4.

We summarize this section by showing the interaction parameters up to second nearest neighbours in the first two bands as a function of R_c for a fixed V_0 [figure 6]. The saturation of matrix elements are clearly visible here as well, and can be explained the same way as we did before. Another feature we have seen as that the off-site matrix elements for the lowest and the first excited bands cross each other. At small R_c , it is the overlap between the MLWFs which determines the off-site couplings and they are larger for first excited band compared to the lowest one. On contrary, at sufficiently large R_c the off-site coupling strength depends on how well it is accommodated inside the soft-core barrier and in that case the lowest band dominates resulting in a crossing between them as a function of R_c . We also noticed that this crossings are even more prominent at small values of V_0 .

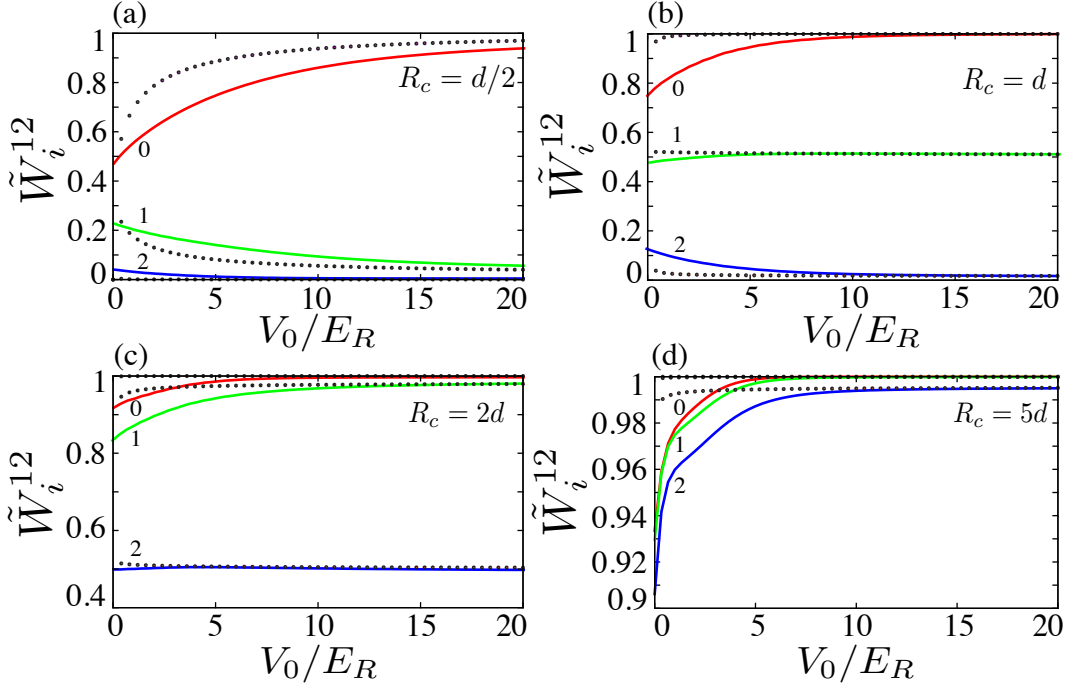


Figure 5. The inter-band matrix elements ($\tilde{W}_i^2 = W_{00ii}^{1122}/W_{eff}$) for the Rydberg admixed interaction as a function of lattice depth V_0 for (a) $R_c = d/2$, (b) $R_c = d$, (c) $R_c = 2d$ and (d) $R_c = 5d$. The results from tight binding approximation are shown by the dotted lines. The value of i is used in labelling the plots.

4.3. Rydberg admixed potential: density assisted tunnelings

We look at the DAT emerging from the Rydberg admixed interactions. Here we show only the two dominant processes [figure 7 (a)] with in the two lowest Bloch bands and found to be explicitly depending on the value of R_c as seen in figure 7 (b). Due to the long range nature of the Rydberg induced potential, the same processes can happen between even far neighbours. Let us first focus on the nearest neighbours, depicted in figure 7 (a). For large R_c , the Rydberg potential can be taken as constant when calculating the amplitudes of these processes which resulting in an integral $\sim \int w_0(x)w_1^*(x)dx \approx 0$, hence you observe a rapid decay for $R_c > d$. Below $R_c < d$, the interactions itself between the sites are weak enough to trigger this processes and hence resulting in a hump like behaviour as a function of R_c . The same matrix elements as a function of V_0 for $R_c = d$ is shown in figure 7 (c). If we consider the same processes between the next nearest neighbours, the above mentioned peak appears at $R_c = 2d$ but with lesser magnitude and so on. Hence we calculated the maximum of the peak as a function inter-particle separation (R_c is changed accordingly) for $V_0 = 10 ER$ [figure. 7 (d)]. Note that all other DAT events are at least one order of magnitude lower than this one. Even though not shown, the scaled amplitude for the process shown in figure fig:uj e(1) due to Rydberg potential is one order of magnitude larger than that from the contact

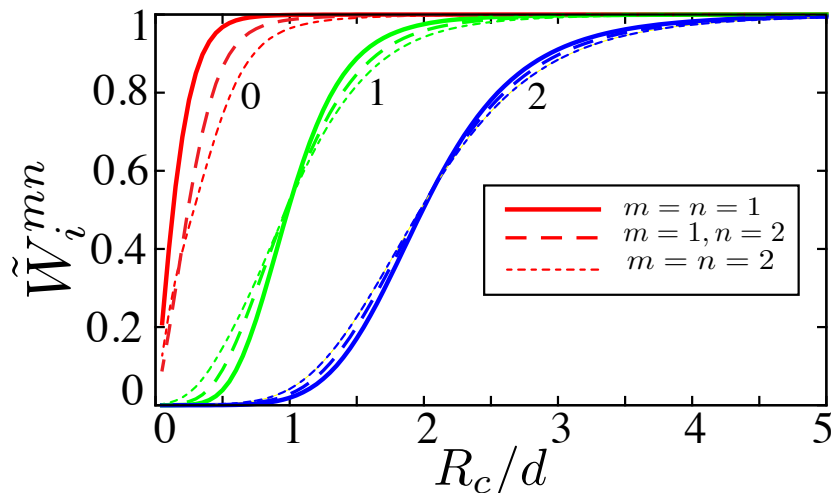


Figure 6. The onsite and off-site matrix elements ($\tilde{W}_i^{mn} = W_{00ii}^{mnnn}/W_{eff}$) for the Rydberg admixed interactions as a function of R_c for $V_0 = 10$. The numbering shown in the plots are for onsite ($i = 0$), nearest neighbour ($i = 1$) and next nearest neighbours ($i = 2$). For each of them the results are shown for the lowest band ($m = n = 1$), first excited band ($m = n = 2$) and between them ($m = 1, n = 2$). For $i = 1$ and $i = 2$ there is a crossing between the parameters for the lowest and the first excited bands.

potential.

4.4. An example: Rubidium atoms

In this session we consider the state of the art Rubidium lattice setup. As we have pointed out earlier in section 4.2, any change in detuning Δ or Ω affect R_c and W_{eff} simultaneously, but R_c can be varied independently by changing the Rydberg states. Below we estimate realistic values for R_c as a function of $C_6(n)$ for Rubidium (^{87}Rb) atoms weakly coupled to $nS_{1/2}$ states, in an 1D optical lattice [figure 8(a)]. We consider a lattice spacing of $d = 391$ nm, which can be achieved using counter propagating laser fields of wavelength $\lambda = 782$ nm. It can be seen that the range of interactions can be extended over as many as 10 sites when considering a Rydberg state $60S_{1/2}$ with $\Delta = 100$ MHz. Note that for fixed C_6 the variation of R_c against Δ is relatively slow. With $\Omega/\Delta = 0.1$ and $\Delta = 100$ MHz, we can attain an effective interaction strength of $W_{eff} = 10$ kHz.

5. Conclusion

In conclusion, we have estimated *ab initio* the Hubbard parameters for Rydberg-dressed atoms in an one-dimensional sinusoidal optical lattice in the basis of maximally localized Wannier states. The finite range, soft-core nature of the Rydberg induced interactions strongly modifies the nature of Hubbard parameters. In particular, in controlling the

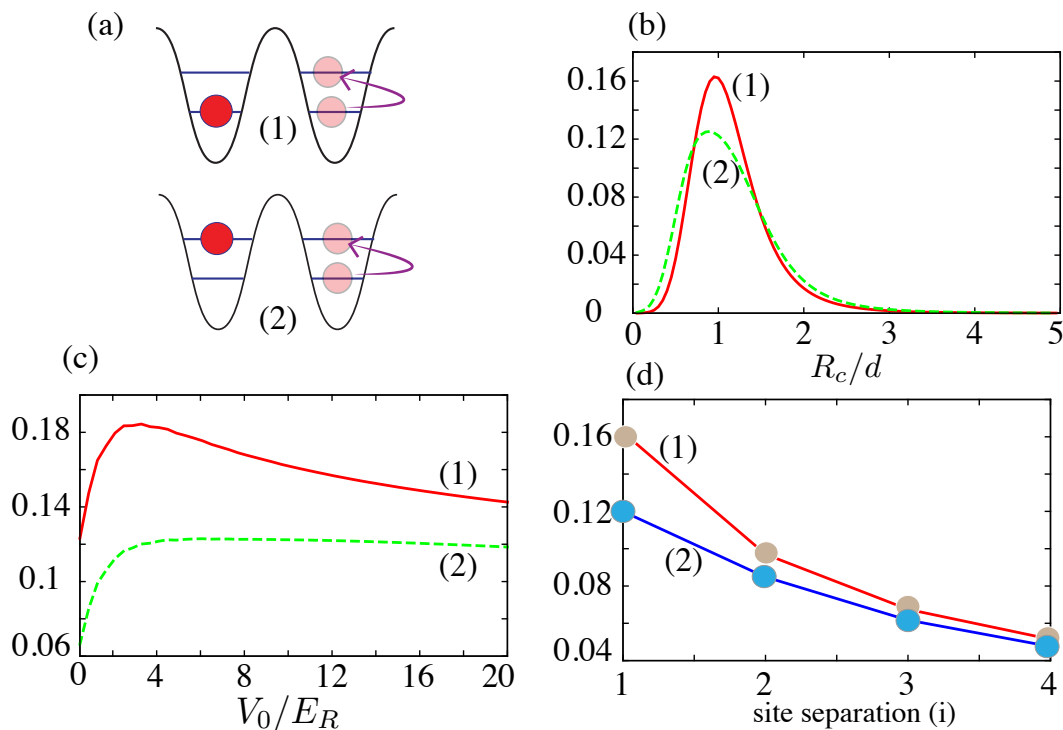


Figure 7. (a) The two dominant off-site DAT processes due to the Rydberg admixed interactions. (b) The amplitudes or strengths of the two events as a function of R_c for $V_0 = 10$ ER. Note that for the nearest neighbour it is peaked at $R_c = d$, and if next nearest neighbours are considered the peak will appear around $R_c = 2d$ but with a lesser magnitude. (c) The same as a function of V_0 for $R_c = d$. (d) The maximum of the peak appearing at different R_c 's as a function of inter-site separation. $i = 1$ means nearest neighbour and so on. The scaled amplitudes (units of W_{eff}) are plotted along the y-axis for figures (b)-(d) and they are labelled by the numbers indicated for the two processes.

spatial extension of the soft-core barrier one can engineer the off-site interactions and make them same magnitude as that of the onsite ones, hence making them position independent. This may influence the many body dynamics in a great deal. In addition to the typical density density interactions, we provide the information for the DAT coefficients in this system. Two dominant process which depends crucially on the soft-core have been identified and discussed which will be highly relevant when studying non-standard multi band Hubbard models. In the end, we have discussed realistic parameters for the state of the art experimental Rydberg dressed Rubidium lattice setup.

6. Acknowledgements

We acknowledge useful discussions with Venkateswara Pai, Prasenjit Ghosh and Umesh Waghmare. R.N acknowledges the funding by the Indo-French Centre for the Promotion

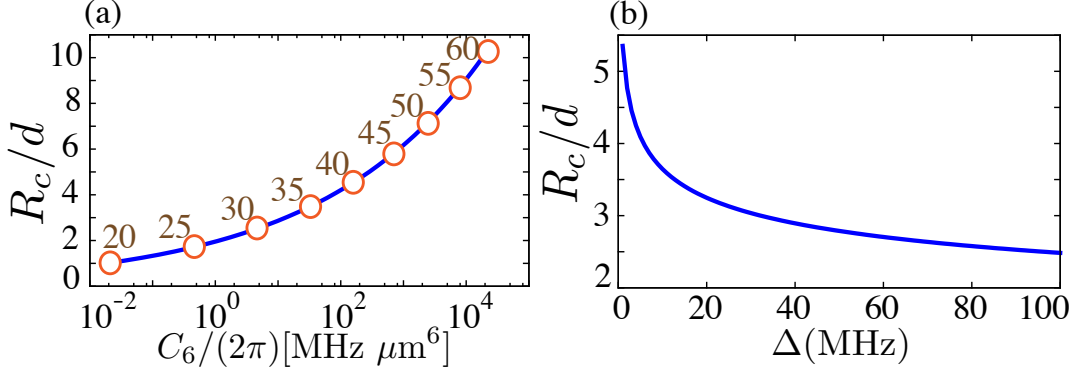


Figure 8. (a) The range of Rydberg admixed interaction (R_c) as a function of $C_6(n)$ for ^{87}Rb atoms in which the ground state is weakly admixed to $nS_{1/2}$ states with a detuning $\Delta = 100$ MHz. The corresponding principal quantum numbers n are indicated by the empty bubbles. (b) R_c as a function of Δ for $30S_{1/2}$.

of Advanced Research (CEFIPRA).

Appendix A. Single particle energy bands and Bloch states in an 1D optical lattice

The Hamiltonian for a single particle in the presence of an 1D optical lattice potential $V(x)$ is

$$\hat{h}_0 = -\frac{\hbar^2}{2m} \frac{d^2}{dx^2} + V(x), \quad (\text{A.1})$$

where $V_{OL}(x) = V_0 \sin^2(k_0 x)$ and the wave number $k_0 = \pi/d$ with d being the lattice spacing. The single particle energy band structure is obtained by solving the eigenvalue equation $\hat{h}_0 \psi_q^n(x) = E_q^n \psi_q^n(x)$ for a given quasi-momentum $q \in [-\pi/d, \pi/d]$ and n is the band index. According to Bloch theorem, we have Bloch solutions $\psi_q^n(x) = e^{iqx} u_n^q(x)$ and $u_n^q(x)$ has the same periodicity as that of the lattice potential. The above eigen value equation is best tackled in the Fourier space, and by introducing the Fourier expansion for the lattice potential $V(x) = (V_0/\sqrt{d}) \sum_k v_k e^{iG_k x}$ and for $u_n^q(x) = (1/\sqrt{d}) \sum_k c_{q,k}^n e^{iG_k x}$. With Fourier coefficients $c_{q,k}^n$ satisfying the normalization condition $\sum_k (c_{q,k}^m)^* c_{q,k}^n = \delta_{m,n}$, the periodic functions $u_n^q(x)$ is normalized over the primitive unit cell of the lattice in the real space. Finally we arrive at

$$\frac{\hbar^2}{2m} (G_k + q)^2 c_{q,k}^n + \frac{1}{\sqrt{d}} \sum_{k'} v_{k-k'} c_{q,k'}^n = E_q^n c_{q,k}^n. \quad (\text{A.2})$$

We can write the above equation in a matrix form as $H_q c_q^n = E_q^n c_q^n$ with eigen vectors c_q^n and eigen values E_q^n . The matrix elements of H_q :

$$(H_q)_{ij} = \frac{\hbar^2}{2m} (G_i + q)^2 \delta_{ij} + \frac{1}{\sqrt{d}} v_{i-j}. \quad (\text{A.3})$$

Diagonalizing H_q provides us the Fourier coefficients $c_{q,k}^n$ and they possess certain properties based on various symmetries. If inversion symmetry exists and together with time-reversal symmetry, they guarantee that $c_{q,k}^n$ are real apart from a common phase factor and also satisfies $c_{q,k}^n = (c_{-q,-k}^n)^*$. This property can considerably reduce the numerical cost in calculating the Bloch functions $\psi_q^n(x)$. We employ a LAPACK routine to obtain the eigen states and eigen values of the Hamiltonian matrix given in equation A.3 for $q \in [-\pi/d, \pi/d]$. The eigen vectors c_q^n are real-valued and the periodic Bloch function $u_q^n(x)$ is then obtained by its Fourier transform.

References

- [1] Santos L, Shlyapnikov G V, Zoller P, and Lewenstein M 2000 *Phys. Rev. Lett.* **85** 1791
- [2] Honer J, Weimer H, Pfau T and Büchler H P, 2010 *Phys. Rev. Lett.* **105** 160404
- [3] Johnson J E and Rolston S L, 2010 *Phys. Rev. A* **82** 033412
- [4] Pupillo G, Micheli A, Boninsegni, Lesanovsky I and Zoller P 2010 *Phys. Rev. Lett.* **104** 223002
- [5] Henkel N, Nath R and Pohl T 2010 *Phys. Rev. Lett.* **104** 195302
- [6] Macrì T and Pohl T 2014 *Phys. Rev. A* **89** 011402
- [7] Balewski J B, Krupp A T, Gaj A, Hofferberth S, Löw R and Pfau T 2014 *New J. Phys.* **16** 063012
- [8] Mukherjee R, Killian T C and Hazzard R A, arXiv:1511.08856
- [9] Saffman M, Walker T G and Molmer K 2010 *Rev. Mod. Phys.* **82** 2313
- [10] Lukin M D, Fleischhauer, Cote R, Duan L M, Jaksch D, Cirac J I and Zoller P 2001 *Phys. Rev. Lett.* **87** 037901
- [11] Urban E, Johnson T A, Henage T, Isenhower L, Yavuz D D, Walker T G and Saffman M 2009 *Nature Phys.* **5** 110
- [12] Gaëtan A, Miroshnychenko Y, Wilk T, Chotia A, Viteau M, Comparat D, Pillet P, Browaeys A and Grangier P 2009 *Nature Phys.* **5** 115
- [13] Pohl T, Demler E and Lukin M D, 2010 *Phys. Rev. Lett.* **104** 043002
- [14] Weimer H, Löw R, Pfau T and Büchler H P 2008 *Phys. Rev. Lett.* **101** 250601
- [15] Löw R, Weimer H, Krohn U, Heidemann R, Bendkowsky V, Butscher B, Büchler H P, and Pfau T 2009 *Phys. Rev. A* **80** 033422
- [16] Weimer H and Büchler H P, 2010 *Phys. Rev. Lett.* **105** 230403
- [17] Olmos B, González-Férez, and I. Lesanovsky 2009 *Phys. Rev. Lett.* **103** 185302
- [18] Ji S, Ates C and Lesanovsky I 2011 *Phys. Rev. Lett.* **107** 060406
- [19] Lesanovsky I 2011 *Phys. Rev. Lett.* **106** 025301
- [20] Jau Y Y, Hankin A M, Keating T, Deutsch I H and Biedermann G W 2015, *Nature Phys.*
- [21] Hsueh C H, Lin T C, Horng T L and Wu W C 2012 *Phys. Rev. A*, **86** 013619
- [22] Cinti F, Jain P, Boninsegni M, Micheli A, Zoller P and Pupillo G 2010 *Phys. Rev. Lett.* **105** 135301
- [23] Li S and Sarma S D 2015 *Nature Comm.* **6** 7137
- [24] Geissler A, Vasic I and Hofstetter W, arXiv:1509.06292
- [25] Maucher F, Henkel N, Saffman M, Królikowski W, Skupin S and Pohl T 2011 *Phys. Rev. Lett.* **106** 170401
- [26] van Bijnen B M W and Pohl T 2015 *Phys. Rev. Lett.* **114** 243002
- [27] Dauphin A, Müller M, and Martin-Delgado M A 2012, *Phys. Rev. A* **86** 053618
- [28] Glaetzle A W, Dalmonte M, Nath R, Rousochatzakis I, Moessner R and Zoller P 2014 *Phys. Rev. X* **4** 041307
- [29] Glaetzle A W, Dalmonte M, Nath R, Gross C, Bloch I and Zoller P 2015 *Phys. Rev. Lett.* **114** 173002
- [30] Keating T, Goyal K, Jau Y Y, Biedermann G W, Landahl A J and Deutsch I H 2013 *Phys. Rev. A* **87** 052314

- [31] Keating T, Cook R L, Hankin A M, Jau Y Y, Biedermann G W, and Deutsch I H 2015 *Phys. Rev. A* **91** 012337
- [32] Möbius S, Genkin M, Eisfeld A, Wster S, and Rost J M 2013 *Phys. Rev. A* **87** 051602(R)
- [33] Gil L I R, Mukherjee R, Bridge E M, Jones M P A and Pohl T 2014 *Phys. Rev. Lett.*, **112**, 103601
- [34] Bouchoule I and Mlmer K 2002, *Phys. Rev. A*, **65**, 041803
- [35] Gaul C, DeSalvo B J, Aman J A, Dunning F B, Killian T C and Pohl T arXiv:1511.06424
- [36] Lewenstein M, Sanpera A and Ahufinger V 2012 *Ultracold atoms in optical lattices: Simulating quantum many body systems* (Oxford University press, New York, 2012).
- [37] Bloch I, Dalibard J, and Zwerger W 2008 *Rev. Mod. Phys.* **80** 885
- [38] Jaksch D, Bruder D, Cirac J I, Gardiner C W and Zoller P 1998 *Phys. Rev. Lett.*, **81**, 3108
- [39] Fisher M P A, Weichman P B, Grinstein G, and Fisher D S 1989 *Phys. Rev. B*, **40** 546
- [40] Greiner M, Mandel O, Esslinger T, Hänsch T W and Bloch I 2002 *Nature*, **415** 39
- [41] Gericke T, Wrtz P, Reitz D, Langen T and Ott H 2008 *Nature Phys.*, **4**, 949
- [42] Bakr W S, Gillen J I, Peng A, Flling S and Greiner M 2009 *Nature*, **462**, 74
- [43] Sherson J F, Weitenberg C, Endres M, Cheneau M, Bloch I and Kuhr S 2010 *Nature*, **467** 68
- [44] Kohn W 1959 *Phys. Rev.*, **115** 809
- [45] Brouder C, Panati G, Calandra M, Mourougane C, and Marzari N 2007 *Phys. Rev. Lett.*, **98**, 046402
- [46] Marzari N and Vanderbilt D 1997, *Phys. Rev. B*, **56**, 12847
- [47] Marzari N, Mostofi A A, Yates J R, Souza I and Vanderbilt D 2012 *Rev. Mod. Phys.*, **84** 1419
- [48] Walters R, Cotugno G, Johnson T H, Clark S R, and Jaksch D 2013 *Phys. Rev. A*, **87**, 043613
- [49] Baranov M, Dalmonte M, Pupillo G, and Zoller P 2012, *Chem. Rev.* **112**, 5012
- [50] Trefzger C, Menotti C, Capogrosso-Sansone B and Lewenstein M 2011, *J. Phys. B: At. Mol. Opt. Phys.*, **44**, 193001
- [51] Scalettar R T, Batrouni G G, Kampf A P, and Zimanyi G T 1995, *Phys. Rev. B*, **51** 8467
- [52] Scarola V W and Sarma S D 2005, *Phys. Rev. Lett.*, **95**, 033003
- [53] Yi S, Li T, and Sun C P 2007, *Phys. Rev. Lett.*, **98**, 260405
- [54] Pollet L, Picon J D, Behler H P, and Troyer M 2010 *Phys. Rev. Lett.*, **104**, 125301
- [55] Capogrosso-Sansone B, Trefzger C, Lewenstein M, Zoller P, and Pupillo G 2010, *Phys. Rev. Lett.*, **104** 125301
- [56] Dalla Torre E G, Berg E, and Altman E 2006, *Phys. Rev. Lett.*, **97** 260401
- [57] Baier S, Mark M J, Petter D, Aikawa K, Chomaz L, Cai Z, Baranov M, Zoller P and Ferlaino F arXiv:1507.03500
- [58] Jürgensen, Meinert F, Mark M J, Nägerl H C, and Lühmann D S 2014 *Phys. Rev. Lett.* **113** 193003
- [59] Mattioli M, Dalmonte M, Lechner W, and Pupillo G 2013 *Phys. Rev. Lett.*, **111** 165302
- [60] Dutta O, Gajda M, Hauke P, Lewenstein M, Lühmann D.-S, Malomed B A, Sowiński T and Zakrzewski J 2015 *Rep. Prog. Phys.* **78** 066001
- [61] Sowiński T, Dutta O, Hauke P, Tagliacozzo T, and Lewenstein M 2012 *Phys. Rev. Lett.* **108** 115301
- [62] He L and Vanderbilt D 2001 *Phys. Rev. Lett.*, **86** 5341
- [63] Edmiston C and Ruedenberg K 1963 *Rev. Mod. Phys.*, **35** 457